Automated analysis of 3D echocardiography

Stralen, M. van

Semi-automatic endocardial border detection for left ventricular volume estimation in 3D echocardiography

2

We propose a semi-automatic endocardial border detection method for LV volume estimation in 3D time series of cardiac ultrasound data. It is based on pattern matching and dynamic programming techniques and operates on 2D slices of the 4D data requiring minimal user-interaction.
We evaluated on data acquired with the fast rotating ultrasound (FRU) transducer: a linear phased array transducer rotated at high speed around its image axis, generating high quality 2D images of the heart. We automatically select a subset of 2D images at typically 10 rotation angles and 16 cardiac phases. From four manually drawn contours a 4D shape model and a 4D edge pattern model is derived. Pattern matching and dynamic programming is applied to detect the contours automatically. The method allows easy corrections in the detected 2D contours, to iteratively achieve more accurate models and improved detections.
An evaluation of this method on FRU data against MRI was done for full cycle LV volumes on 10 patients. Good correlations were found against MRI volumes ($r = 0.94$, $y = 0.72x + 30.3$, a difference of 9.6 ± 17.4 ml (mean $\pm$ standard deviation)) and a low interobserver variability for 3DE ($r = 0.94$, $y = 1.11x - 16.8$, difference of 1.4 ± 14.2 ml). On average only 2.8 corrections per patient were needed (in a total of 160 images). Although the method shows good correlations with MRI without corrections, applying these corrections can make significant improvements.

This chapter has been derived from (© 2005 SPIE):
Semi-automatic border detection method for left ventricular volume estimation in 4D ultrasound data. M. van Stralen, J.G. Bosch, M.M. Voormolen, G. van Burken, B.J. Krenning, R.J.M. van Geuns, E. Angelié, R.J. van der Geest, C.T. Lancée, N. de Jong, J.H.C. Reiber. Proc SPIE Med Imaging 2005; 5747; 1457-1467.

2.1 | Introduction

3D echocardiography

For diagnosis of cardiovascular diseases, the volume and ejection fraction of the left heart chamber are important clinical parameters. 3D echocardiography (3DE) offers good opportunities to visualize the whole left ventricle (LV) over the complete cardiac cycle. 3D echocardiography is non-invasive, relatively cheap, flexible in use and capable of accurate volume measurements [Jenkins et al. 2004; Nosir et al. 1999]. New, fast 3D ultrasound imaging devices are entering the market and have the potential of allowing such measurements rapidly, reliably and in a user-friendly way - provided that a suitable automated analysis is available. Manual segmentation of the large data sets is very cumbersome and suffers from inconsistencies and high variability. On the other hand, the human expert's interpretation and intervention in the detection is often essential for good results. Therefore a semi-automatic segmentation approach seems most suitable.

2.1.1 | Other approaches

Some methods for segmentation of 3D echocardiographic images have been published. Angelini et al. [2001] have reported on a wavelet-based approach for 4D echocardiographic image enhancement followed by a segmentation of the left ventricle using snakes. Corsi et al. [2002] presented a level-set based semi-automatic method. Montagnat and Delingette [2000] used a 2-simplex mesh and a feature detection based on a simple cylindrical gradient filter. Sanchez-Ortiz et al. [2002] used multi-scale fuzzy clustering for a rough segmentation in 2D longitudinal slices. B-splines are used for 3D surface fitting in each time frame. These methods have not been validated successfully on a reasonable data set. The most practical approach is described by Kühl et al. [2004]. It uses active surfaces that are controlled by difference-of-boxes operators applied to averages and variances of the luminance. This technique is implemented in a commercially available workstation (4D LV Analysis, TomTec, Unterschleißheim, Germany). The general experience is that this technique requires much initialization and corrections, and a consistent segmentation is still hard to reach. Another commercial development has been presented recently: QLAB (Philips Medical Systems, Best, the Netherlands). This package provides on- and offline 3D quantification tools. However, technical details or clinical evaluations of these methods have not been reported yet.

our approach

We present a semi-automatic endocardial border detection method for left ventricular volume estimation in time series of 3D cardiac ultrasound data.Our method is based on pattern matching and dynamic programming techniques and com-

Figure 2.1: The fast rotating ultrasound (FRU) transducer

bines continuity, robustness and accuracy in 2D cross sections with the spatial and temporal continuity of the 3D plus time (3D+T) data. It aims at optimally using a limited amount of user interaction (capturing essential information on shape and edge patterns according to the user's interpretation of the ultrasound data) to attain a fast, consistent and precise segmentation of the left ventricle.

Despite the fact that this method is optimized for data of the fast rotating ultrasound transducer (see below), the algorithm can be easily adapted to data of other image acquisition systems, for example 3D+T voxel sets. The detection will then be performed in 2D slices through the LV long axis.

general applicability

Fast rotating ultrasound transducer | 2.1.2

We performed this study on a special type of image data acquired with a new device: the fast rotating ultrasound (FRU) transducer (fig. 2.1). The transducer has been developed by the Department of Experimental Echocardiography of the Erasmus MC, the Netherlands [Djoa et al. 2000; Voormolen et al. 2002]. It contains a linear phased array transducerthat is continuously rotated around its image axis at very high speed, up to 480 rotations per minute (rpm), while acquiring 2D images. A typical data set is generated during 10 seconds at 360 rpm and 100 frames per second (fps). The images of the left ventricle are acquired with the transducer placed in apical position, with the transducer's rotation axis more or less aligned with the LV long axis. The analysis assumes that the rotation axis lies within the LV lumen and inside the mitral ring.

linear phased array transducer

An important advantage of this transducer is that it can be used with any ultra-

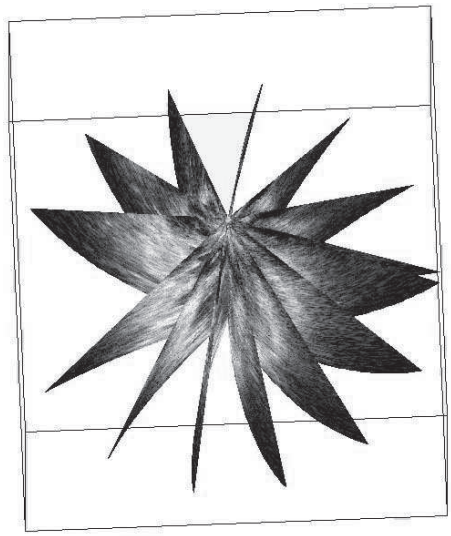

Figure 2.2: A sequence of seven consecutive FRU images with curved image planes

usage with any ultrasound machine

sound machine, since a conventional phased array transducer is used. It also acquires relatively high quality 2D images, compared to matrix array transducers used for real-time 3D echocardiography. Furthermore, no ECG triggering is applied, just an ECG-registration for offline analysis, which allows quick acquisitions.

As a consequence of the very high continuous rotation speed, the images have a curved image plane (fig. 2.2). During the acquisition, the probe rotates about 22° per image with the typical settings given above. The combination of these curved image planes, and the fact that the acquisition isnot triggered by or synchronized to the ECG signal, results in an irregular distribution over the 3D plus time (3D+T) space. A single cardiac cycle in general is not sufficient for adequate coverage of the whole 3D+T space; therefore, multiple consecutive heart cycles are merged. The cardiac phase for each image is computed offline using detected R-peaks in the ECG [Engelse and Zeelenberg 1979]. From the total set of ±1000 2D images, a subset of images with a regular coverage of the 3D+T space is selected automatically. We perform analysis on the images in this subset. The data is also suitable for the generation of a time series of 3D voxel sets.

acquisition is not ECG triggered

Methods | 2.2

Frame selection | 2.2.1

To achieve adequate coverage of the whole 3D+T space, multiple consecutive cardiac cycles are merged and an optimal subset S of the total set of frames T is selected (fig. 2.3). This subset is an optimal fit of the frames on a chosen $A \times P$ matrix of A equidistant rotation angles and P cardiac phases, minimizing the total deviation in rotation angle and cardiac phase.Moreover, the variation in acquisition time over the subset is minimized to limit possible motion artifacts. The constraints are translated into the following cost functions that will be minimized over the total subset S,

limit motion artifacts

$$S = \bigcup_{i=1}^{A} \bigcup_{j=1}^{P} (\underset{b \in C_{i,j}}{\arg\min}(c_{\text{angle}}(\alpha_b, i) + c_{\text{phase}}(p_b, j) + c_{\text{time}}(t_b))) \tag{2.1}$$

$$c_{\text{angle}}(\alpha, i) = k_1 |\alpha_{\text{target}}(i) - \alpha|$$

$$c_{\text{phase}}(p, j) = k_2 |p_{\text{target}}(j) - p|$$

$$c_{\text{time}}(t) = k_3 |t_S - t|$$

$C_{i,j}$ is the set of candidate images for angle $\#i$ and phase $\#j$. c_{angle} and c_{phase} describe the costs of selecting an image b with angle α_b and phase p_b for a chosen α_{target} and p_{target}. k_1, k_2 and k_3 are weighting coefficients (typically equal). Since the cost c_{time} is dependent on t_S (the average acquisition time of the subset itself), the minimization of the costs of set S is achieved in an iterative manner.

iterative frame selection optimization

Border detection approach | 2.2.2

We base our method on the knowledge that the edge patterns of the endocardial border can be complex, very different from patient to patient and even between regions within an image set. The border position need not correspond to a strong edge and may be only definable from 'circumstantial evidence' as identified by an expert observer. Rather than applying artificial, idealized edge models or templates derived from a large training set, we propose a tracking approach based on edge templates extracted from the user-defined initial borders in the patient's own images.

patient specific edge template

The method is based on the following continuity assumptions (in order of strength):

(a) border continuity within separate 2D slices of the left ventricle;

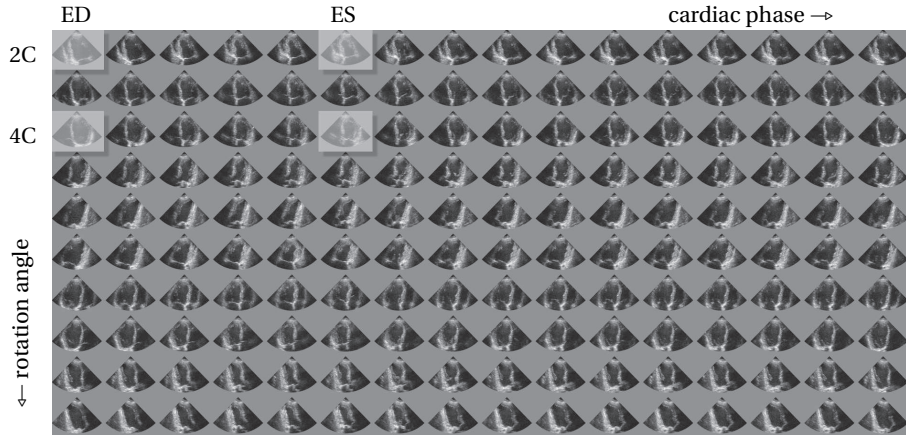

Figure 2.3: Selected subset of 2D FRU images in 16 cardiac phases and 10 rotation angles. Contours are manually drawn in the highlighted images.

(b) spatial continuity of shape and gray value edge patterns over the LV surface in 3D;

(c) temporal and cyclic motion continuity of the endocardium.

For the FRU transducer, within the original 2D images, both spatial and temporal distances between neighboring samples are smaller than towards adjacent images in angle and phase; therefore, border continuity is supposed to be strongest here.

manual initialization

The method is initialized from four manually drawn contours, taken from two roughly perpendicular views (more or less corresponding to two- and four-chamber cross sections) in two phases: end diastole (ED) and end systole (ES). These are used to initialize a model for the edge patterns near the 3D LV surface over time and a 3D shape model of the LV endocardial surface over the entire cardiac cycle. Both models are inherently 4-dimensional and can be polled at any spatial position and cardiac phase.

method overview

The actual border detection takes place in individual 2D images from the selected subset and is an extension of an approach for 2D+T sequences earlier developed by Bosch et al. [1998]. For each image $b \in S$ (of cardiac phase p_b and rotation angle α_b), an estimation of the border shape is derived by intersecting the 3D shape model at phase p_b by the (curved) image plane for angle α_b. The edge templates are also interpolated for the desired p_b and α_b. In the 2D image, a neighborhood of the estimated shape is resampled along lines perpendicular to the shape estimate. Using a template matching with the local edge templates, the similarity of

each candidate edge point to the template is calculated. Dynamic programming is applied to find an optimal continuous border within the restrictions posed by the 3D model. In this way, the 3D+T surface and edge pattern models guard the (looser) spatial and temporal consistency of the detection, while the dynamic programming approach supplies a continuous and optimal detection locally. The set of detected contours describes the 3D endocardial surface over the whole cardiac cycle from which LV volumes, ejection fraction and other valuable parameters can be computed.

3D surface models | 2.2.3

Definition | 2.2.3.1

As said, for two cardiac phases (ED and ES) a 3D surface model of the LV endocardium is constructed from two almost perpendicular contours. During the acquisition the rotation axis is more or less aligned with the long axis (LAX) of the left ventricle, but in practice there may be a considerable mismatch (fig. 2.4b). This implies that the two image planes do not contain the true apex of the left ventricle, and estimating the position and shape of the true apex (and the LV long axis) is a non-trivial issue. The local long axes in the 2D manually drawn contours are defined as the lines through the midpoint of the mitral valve (MV) and center of gravity of the upper 10% of the contour area. We estimate the 3D LV long axis from the local long axes by computing the intersection of the planes perpendicular to these images through the local long axis in the image.

manual contours miss apex

The endocardial surface is estimated by expressing the two contours in a cylindrical coordinate system with respect to the estimated LV long axis. Intersection points of these contours are found with a stack of planes perpendicular to the long axis (short-axis planes). Within each short-axis plane, a closed contour is found by interpolating between the intersection points; for this, the radial coordinate component r is interpolated over the angle between the intersection points (see section 2.2.3.2 for details). This gives a natural approximation of the ellipsoidal shape of the left ventricle. Since the two image planes generally do not intersect the real apex, the apical cap of the LV surface cannot be estimated simply from the two manually drawn contours, as shown in fig. 2.4b. Therefore, near the 3D apex we use a spherical coordinate system oriented around the LV long axis, centered at $3/4^{\text{th}}$ of its length. The surface is estimated by interpolating the radial component over the elevation angle for multiple rotation angles, using the interpolation method described in the next section. A contour estimate for any 2D image at a given rotation angle and cardiac phase can be made by intersecting its curved image plane with

shape models in ED and ES

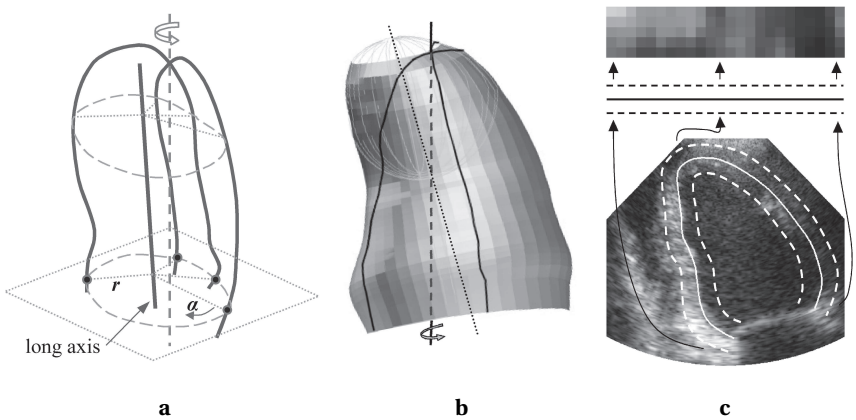

Figure 2.4: *a*) The interpolation of the endocardial surface in a cylindrical coordinate system oriented around the LV long axis (LAX). *b*) 3D surface model. The LAX estimate (dotted) and the rotation axis (dashed) are shown, together with the reconstruction of the apex by spline interpolation (light gray) from two manually drawn contours (solid black). *c*) The extraction of a stylized edge pattern from an image with a manually drawn contour.

the 3D contour models in ED and ES and then linearly interpolating between the two resulting '2D' contours over cardiac phase to get the contour estimate at the desired cardiac phase.

2.2.3.2 | Surface interpolation/fitting

Fitting a smooth contour through all available intersection points in a short-axis plane is not always possible. Inconsistencies can occur in the set of input contours used for the interpolation of the endocardial surface interpolation. They can be caused by inconsistent manual tracing or by inconsistent image data. The latter can be caused by substantial differences in cardiac phase between the images or by inter-beat variation. For the generation of a smooth endocardial surface, we developed a fitting algorithm that can handle these inconsistencies.

dynamic programming

The algorithm is dynamic programming based. Dynamic programming (DP) [Sonka et al. 1999] is a well known graph search technique that finds the optimal path through a rectangular array of nodes (the path with the lowest sum of costs) out of all possible connective paths in an effective manner by calculating lowest cumulative costs for consecutive layers (lines) while keeping track of the partial optimal paths. Backtracking from the node with lowest cumulative cost in the last

layer delivers the overall optimal path. A connective path contains exactly one node per line and the positions on consecutive lines cannot differ more than a predefined side step size.

Using this technique, the method fits an optimal curve through a set of possibly inconsistent intersection points. It allows the assignment of reliabilities to each point.Also, the curvature can be controlled through parameters in the dynamic programming algorithm and the probability distribution computation, which is explained below.

control the curvature

The curve is found through the set of intersection points $i \in I$ with corresponding reliabilities p_i. The nodes in the DP array of size $A \times R$, represent points in (α, r)-space. Finding the path with the minimum costs solves the fitting problem. The costs of each node are represented by the cost function C,

$$C(n) = -\log(P^*(n)), \tag{2.2}$$

where $P^*(n)$ is the normalized probability that node n represents a point on the endocardial border. The normalization is performed within each layer of the DP graph, such that the probabilities within each layer sum up to one. The probability $P(n)$ of node n being part of the endocardial border is inversely related to the angular and radial distance to the intersection points, δ_α and δ_r, and is defined as,

$$P(n) = p_0 + \sum_{i \in I} p_i G(\delta_r, \sigma) \tag{2.3}$$

$$\sigma = c_1(\delta_\alpha + c_2)^{c_3} \tag{2.4}$$

The probability distribution is Gaussian (G) in the radial direction (within the DP layers), as defined in eqn. 2.3. The width of the Gaussian increases with the angular distance from the input point δ_α (eqn. 2.4), which makes the distribution more flat with increasing angular distance. c_1, c_2 and c_3 are parameters that influence the curvature and smoothness of the resulting curve, where $c_1 > 0$, $c_2 > 0$ and $c_3 > 1$. An example cost matrix and the resulting curve are shown in fig. 2.5.

Edge pattern model | 2.2.4

The desired edges are tracked over space and time by applying a pattern matching approach with edge templates.These edge patterns are derived from the manually drawn contours and interpolated over the (phase, angle)-space. The image is resampled clockwise along the manually drawn contour, on line segments perpendicular to this contour from the inside out. The gray values on these line segments are smoothed and subsampled to form a stylized edge pattern for this contour (fig.

derived from manual contours

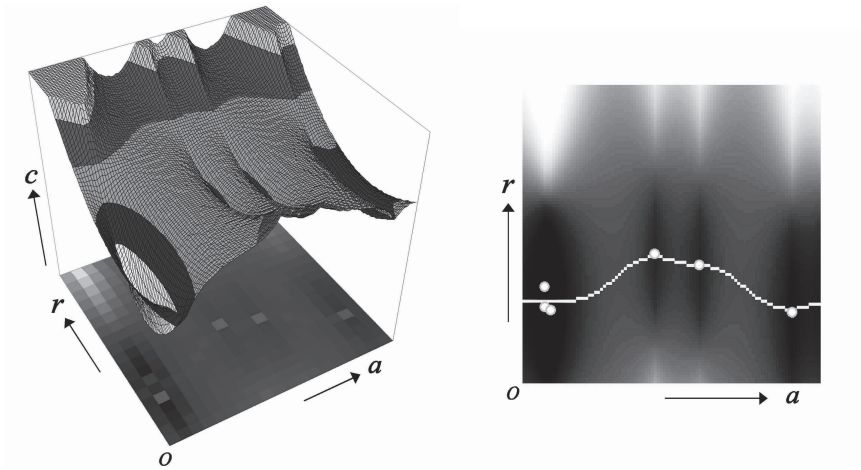

Figure 2.5: *a*) The dynamic programming cost matrix. *b*) The resulting curve fit through the input piont

2.4c). A typical edge pattern for a single 2D frame is represented by 32 positions along the contour and 5 samples around each edge position.

interpolation over rotation angle

The interpolation over cardiac phase is performed linearly between the edge patterns in ED and ES. The interpolation over rotation angle is less straightforward. Since the character of the edge pattern is strongly related to the angle between the endocardial border and the ultrasound beam and the distance from the transducer, the pattern changes considerably over the rotation angle, especially when the angle between the rotation axis and LV long axis is substantial. For images with rotation angles opposite (±180°) to those with the manually drawn contours, the image appears nearly mirrored and the mirrored (anti-clockwise) edge pattern is used. For angles in between, the edge patterns are linearly interpolated.

2.2.5 | Contour detection

image resampling

With an edge pattern and initial contour for each image $b \in S$ (of phase p_b and angle α_b), we can now detect the individual endocardial borders (fig. 2.6). In a neighborhood of the initial contour, the image isresampled into an $N \times M$ rectangular array by sampling N points along M scan lines perpendicular to the shape. From the styl-

ized edge pattern for (p_b, α_b) an edge template for each scan line is extracted. For all nodes in the array, the sum of absolute differences with its respective edge template defines the cost of the node.We now use a dynamic programming approach (section 2.2.3.2, [Sonka et al. 1999]) to find the optimal connective path through the array. Smoothness constraints are enforced by applying additive costs for side stepping during cumulative cost calculation. To limit the influence of lines with relatively poor image information, this additive penalty is calculated per line from the statistics of node costs per line with respect to overall cost statistics, such that relatively unreliable lines get higher penalties for side stepping.

dynamic programming

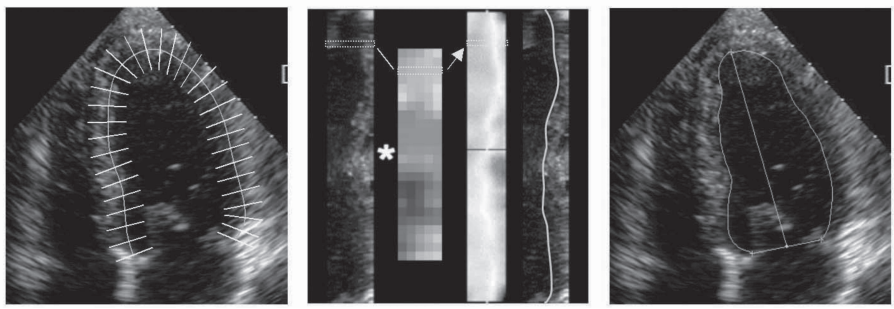

a **b** **c**

Figure 2.6: Contour detection. *a*) Resampling of the image around the 2D shape estimate. *b*) Edge pattern matching and dynamic programming to detect the optimal contour. *c*) The detected contour

For each phase p_j, the detected contours of all angles α_i together constitute a 3D mesh that describes the endocardial surface. We observe the volume of the left ventricle over the whole cardiac cycle, by calculating the volumes inside the surface meshes of all selected cardiac phases.

Correct and redetect | 2.2.6

In the initial detection the shape and edge pattern models are estimated from only four manually drawn contours. In some cases, this does not provide enough information for the models to detect the endocardial border well in all the images in the subset. Also, the border may be poorly defined in some of the images, which complicates the detection. Therefore the method allows additional corrections in the detected contours in the 2D images. A corrected contour will be treated as an

iterative refinements

additional manual contour and both the edge pattern and shape models will be updated accordingly, achieving a more specific approximation of the actual shape and appearance. This results in a new set of shape and edge pattern estimates, and all remaining images are redetected. Through these easy, iterative refinements, corrections will cumulatively lead to a superior global solution.

2.3 | Results

We performed a preliminary validation study for this method on a group of 10 subjects with different diagnoses of cardiovascular disease. Full cycle MRI LV volumes on these patients were determined in parallel with the 3DE study, using semi-automatic segmentation tools (MRI-MASS, Medis medical imaging systems, Leiden, the Netherlands) by an independent observer unaware of the 3DE analyses. For the 3DE study, for all patients, subsets of images were created with $P = 16$ phases and $A = 10$ angles. After establishing equivalent tracing conventions, two observers individually analyzed all subsets. We evaluated the semi-automatic segmentation method using only the initial four manually drawn contours, and after applying corrections iteratively.

comparison with MRI

Reading and converting the data and the automated selection of the subset took 7 minutes per patient on average. After the drawing of the four contours, the fully automated detection of the other 156 contours took approximately 60 seconds per patient (Pentium IV 2.6GHz, 2GB RAM). Some examples of manual and detected contours are shown in fig. 2.7. Corresponding endocardial surfaces for all phases are shown in fig. 2.8. From the analyses of both observers, interobserver variabilities of full cycle volumes and ejection fractions (EF) were determined, as well as averages that were correlated to full cycle MRI volumes, both for the situation with and without applying corrections.

analysis time

Results of 3DE (average of the two observers) vs. MRI are shown in table 2.1 and fig. 2.9a-d. Fig. 2.9a shows the full cycle volumes without corrections. A good correlation of $r = 0.92$ was found between MRI and 3DE volumes without corrections. Regression was $y = 0.675x + 32.9$. In general, ED volumes were underestimated by 3DE, while ES volumes were slightly overestimated. Overall the MRI volumes were slightly larger (14.1 ± 19.6 ml (mean $\pm$ standard deviation)). Similar differences between 3DE and MRI volumes have been reported in many studies and can be attributed to differences in tracing conventions between MRI and 3DE. EF results showed a reasonable overall difference of $6.2 \pm 8.9\%$, but the regression was similarly affected ($y = 0.36x + 25.8\%$, $r = 0.63$). For the 3DE interobserver variabil-

without corrections

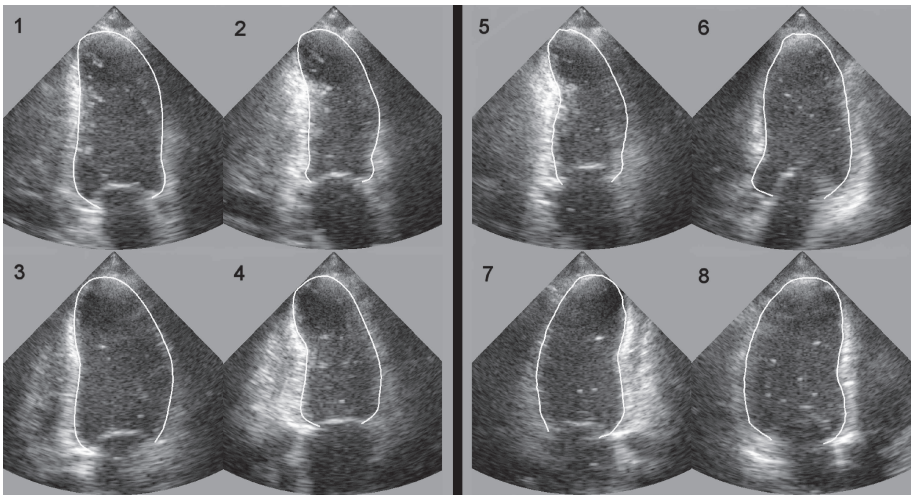

Figure 2.7: Detection examples: frames at different (phase#, angle#) with contours. *left*) 4 frames with manual contours, resp. 1: ED 2c (1,1), 2: ES 2c (6,1), 3: ED 4c (1,3), 4: ES 4c (6,3). *right*) 4 frames with detected contours, resp. 5: frame (8,2), 6: (14,5), 7: (4,8), 8: (14,9)

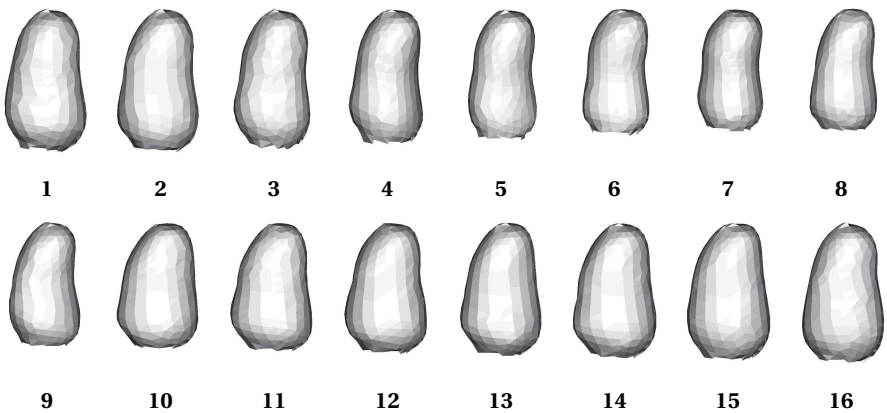

Figure 2.8: Reconstruction of the endocardial border over the full cardiac cycle. The top row shows phases 1 to 8, the bottom row phases 9 to 16 (of a total of 16 phases).

ity, results are presented in table 2.1 and fig. 2.9e. The differences were 5.0 ± 13.6 ml with a regression of $y = 1.08x - 16.0$ ($r = 0.94$).

with corrections

After applying corrections, the full cycle results slightly improved in comparison to MRI volumes: $r = 0.94$, $y = 0.73x + 30.3$, with a difference of 9.6 ± 17.4 ml (table 2.1, fig. 2.9b,d). This is equally reflected in EF results: $r = 0.64$, $y = 0.36x + 25.8$ with differences of $6.0 \pm 8.8\%$. On average 2.8 corrections were applied per patient (on a total of 160 images). Interobserver variability (fig. 2.9f) increased slightly due to the additional corrections, with a correlation of $r = 0.94$ and $y = 1.11x - 16.8$ (difference of 1.4 ± 14.2 ml).

Table 2.1: Full cycle volumes and correlations of 3DE vs. MRI and Observer 1 vs. Observer 2 (N = 160)

		Volume (ml)	**Correlation**	**Regression**
Without corrections	**MRI**	148 ± 48	0.919	$0.675x + 32.9$
	3DE	134 ± 36		
	Obs.1	136 ± 34	0.941	$1.08x - 16.0$
	Obs.2	131 ± 39		
Without corrections	**MRI**	148 ± 48	0.936	$0.728x + 30.3$
	3DE	138 ± 38		
	Obs.1	139 ± 35	0.943	$1.11x - 16.8$
	Obs.2	138 ± 41		

The volumes are expressed as mean ± standard deviation.

2.4 | Discussion

The findings in this study suggest that the semi-automated detection method is a useful tool for quick, semi-automatic detection of LV endocardial borders. However, apparent difficulties in interpreting the 3DE images somewhat obscure the conclusions. Although the different observers can easily reach a satisfactory analysis of the 3DE datasets, the volumetric results show considerable interobserver differences. On inspection, these differences were primarily due to different image

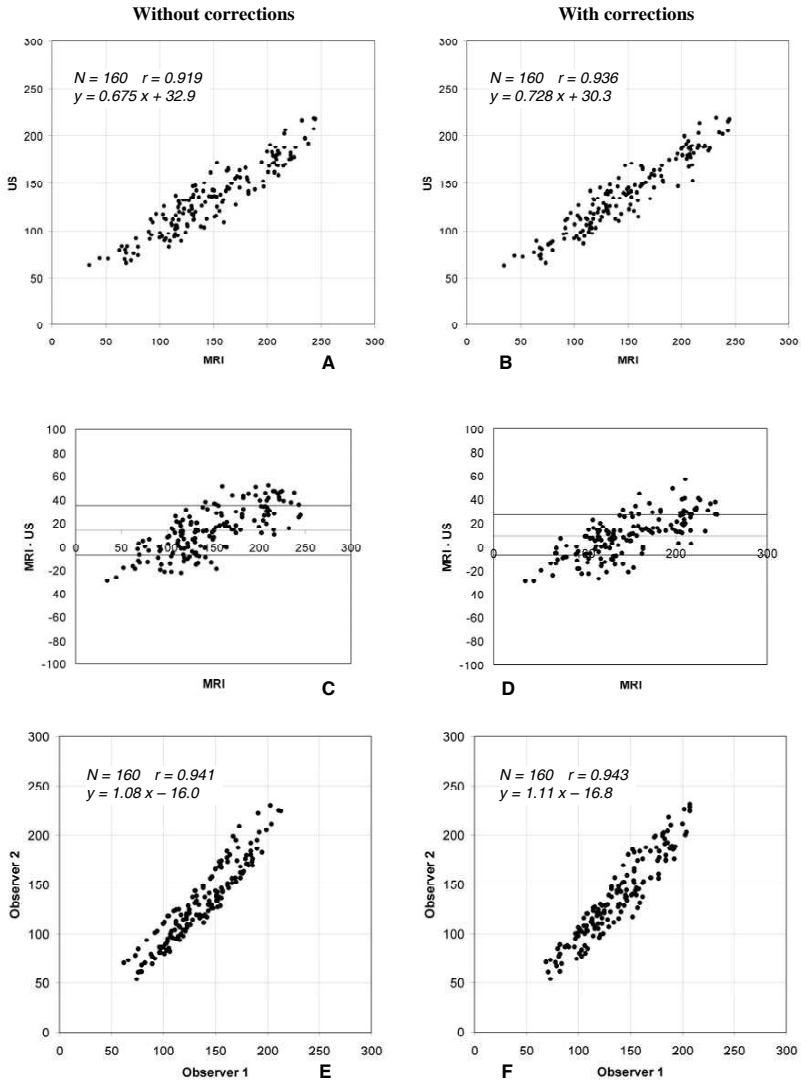

Figure 2.9: All volumes in ml. *a*) MRI vs. 3DE (average of two observers) volumes, without corrections. *b*) MRI vs. 3DE (average of two observers) volumes, with corrections. *c*) Bland-Altman analysis for MRI vs. 3DE, without corrections. *d*) Bland-Altman analysis for MRI vs. 3DE, with corrections. *e*) Interobserver variability (for 3DE), without corrections. *f*) Interobserver variability (for 3DE), with corrections

interpretation and corresponding manual contours, not to differences in detected contours; these consistently followed the observer's interpretation. Clearly, criteria for tracing were not established well enough in this case. This was partly due to the somewhat unconventional cross sections for tracing, partly to the attempt to trace 'similar to MRI criteria' which was not completely successful and meant that we had to deviate from standard ultrasound contour drawing conventions. In some cases, image quality was a factor as well.

Absolute differences in volumes may seem high, but this is partially due to the dilated hearts in the set and the consequent high average volumes (mean MRI ED volume = 187 ml).

tracing conventions

It would be useful to extend the study with tracings following normal ultrasound conventions. This could lead to lower observer variabilities, although the comparison to MRI volumes could be more complicated. Comparison between 3DE and MRI volumes was hampered by the different tracing conventions; this resulted in considerable systematic differences, which were also clearly dependent on cardiac phase. Still, overall regression coefficients were high, especially considering the large interobserver variations for ultrasound. This suggests that with proper tracing conventions and/or correction formulae, a high correspondence between MRI and 3DE volumes should be realizable.

Currently, EF measurements by the 3DE method suffer considerably from the systematic differences and variabilities described above. EF measurements should also benefit greatly from improved tracing conventions.

mitral valve tracking

Looking at the distribution of volume errors over the full cardiac cycle, a shortcoming of this method becomes clear: the lack of a true mitral valve tracking algorithm. Currently, the method simply assumes the movement of the mitral valve to be linear in systole and diastole, which is a substantial simplification. It is well known that the valve plane motion is directly related to LV volume change, and we clearly observe the effect: volume curves which are a bit too 'linear' in diastole and systole. Despite the possibility to adjust this movement using corrections, still high differences can be observed in early systole and diastole in comparison to MRI volume curves. Extending this method with a mitral valve tracking algorithm is expected to further improve the results. Several approaches for mitral valve tracking have already been presented in literature. We elaborate on this topic in chapter 3.

Conclusions and future work | 2.5

We presented a new semi-automatic endocardial border detection method for 3D+T ultrasound data. This method offers fast and reasonably precise automated border detection with minimal user interaction. The method shows good full cycle results against MRI in the initial detections with only four manually drawn contours. After applying corrections, the results do improve for the individual patients, but in the overall comparison against MRI these improvements do not make a significant difference. This can be addressed to the different interpretation of the 3DE data by the observers in comparison to the MRI data. A satisfying detection in 3DE does not always result in equivalent volumes.

The method can still be improved by including a mitral valve tracking algorithm. Furthermore, better tracing conventions for this type of 3DE data would be helpful for consistent analysis.